

## Corrosion behavior of Fe<sub>3</sub>Al intermetallics with addition of lithium, cerium and nickel in 2.5 % SO<sub>2</sub>+N<sub>2</sub> at 900 °C<sup>(\*)</sup>

A. Luna-Ramírez\*, J. Porcayo-Calderón\*, A. Martínez-Villafane\*\*, J. G. González-Rodríguez\*\*\*  
and J. G. Chacón-Nava\*\*

**Abstract** The corrosion behavior of Fe<sub>3</sub>Al-type intermetallic alloys with addition of 1 at. % cerium, lithium and nickel at high temperature has been studied. The various alloys were exposed to an environment composed of 2.5 % SO<sub>2</sub>+N<sub>2</sub> at 900 °C for 48 h. For all the intermetallic tested, the corrosion kinetics showed a parabolic behavior. The alloy, which showed less corrosion rate, was the Fe<sub>3</sub>AlNi alloy, being Fe<sub>3</sub>AlCeLi the alloy with the highest corrosion rate. For the various alloys, energy dispersive X-ray spectroscopy analysis, EDS, on the developed scale only detected aluminum, oxygen, and traces of iron and cerium, suggesting the formation of alumina as main component. The intermetallic alloys showed oxide cracking and spalling. The intermetallic chemical composition played an important role in defining the oxide scale morphology and the extent of damage.

**Keywords** Iron aluminides; Alloy addition; High temperature corrosion; Oxide scale; Oxide/Alloy interface.

## Comportamiento a la corrosión de intermetálicos Fe<sub>3</sub>Al con adición de litio, cerio y níquel en 2,5 % de SO<sub>2</sub>+N<sub>2</sub> a 900 °C

**Resumen** Se estudió el comportamiento a la corrosión a alta temperatura de intermetálicos tipo Fe<sub>3</sub>Al con adición de 1at. % de cerio, litio y níquel. Las diferentes aleaciones fueron expuestas bajo un ambiente compuesto de 2,5 % SO<sub>2</sub>+N<sub>2</sub> a 900 °C durante 48 h. Para todos los intermetálicos ensayados, la cinética de corrosión presentó un comportamiento parabólico. La aleación que mostró la menor velocidad de corrosión fue el intermetálico Fe<sub>3</sub>AlNi, siendo el intermetálico Fe<sub>3</sub>AlCeLi el de mayor velocidad de corrosión. Los análisis mediante espectroscopía de dispersión de rayos X, EDS, sobre la costra formada identificaron únicamente aluminio, oxígeno y trazas de hierro y cerio, lo que sugiere la formación de alúmina como el componente principal. Los intermetálicos mostraron agrietamiento y desprendimiento de la costra de óxido. La composición química de los intermetálicos tuvo un papel importante en la definición de la morfología del óxido formado y el grado de daño.

**Palabras clave** Aluminuros de hierro; Adición de aleantes; Corrosión a alta temperatura; Costra de óxido; Interfase óxido/aleación.

### 1. INTRODUCTION

Materials exposed to an oxidizing environment at high temperatures can suffer corrosion through direct reaction with the gas, without the necessity of a liquid electrolyte. This type of corrosion is known as dry corrosion or high temperature corrosion. The rate of attack might increase substantially as function of temperature. In sulfur-bearing atmospheres, the sulfidation process in gas phase at high temperatures might turn as oxidation process that follows similar

formation mechanisms, growth and evolution of the formation layer<sup>[1]</sup>.

Structural materials based on Fe-Al intermetallic alloys find applications in process industries and power generation systems as structural materials or as cladding for conventional engineering alloys<sup>[2 and 3]</sup>.

Regarding the Fe-Al system, one interesting material is the Fe<sub>3</sub>Al. As with most metallic materials, corrosion resistance is generally imparted by in-situ development of alumina, silica or chromia scales on the alloy surface. The slower the growth rate of the

<sup>(\*)</sup> Trabajo recibido el día 16 de septiembre de 2011 y aceptado en su forma final el día 16 de marzo de 2012.

\* Instituto de Investigaciones Eléctricas Av. Reforma 113, Col. Palmira 62490 Temixco, Morelos, México.  
E-mail: aluna@iie.org.mx.

\*\* CIMAV, Miguel de Cervantes 120, Chihuahua, Chih., México. Tel: 614-4391157. Fax: 614-4391158.

\*\*\* Universidad Autónoma del Estado de Morelos, CIICAP, 62210- Cuernavaca, Mor., México.

oxide, the better alloy oxidation resistance. Of course, other factors such as adequate scale ductility and adherence to the substrate are important. Thus, alumina scales, with slower growth rates as compared with chromia scales can offer substantial advantages in particular for exposures in single-oxidant environments. The oxide scale also act as barriers to the transport of corrosion accelerating reactants such as sulfur, chlorine, and alkalis, and they retard the scaling kinetics of the underlying substrate alloy in multioxidant environments. The oxidation resistance of iron aluminides depends on the formation of a chemically stable  $\text{Al}_2\text{O}_3$  surface layer upon exposure to an oxidizing environment. Studies of the phase stability in the Fe-Al-O system demonstrate that  $\text{Al}_2\text{O}_3$  will form on the iron aluminide class of alloys even at low oxygen partial pressure  $p(\text{O}_2)$ . The aluminum levels (15.9 and 20-30 wt. % in  $\text{Fe}_3\text{Al}$  and FeAl, respectively) present in iron aluminides are well in excess of the critical concentration needed for the formation of a continuous alumina scale on the surface<sup>[4]</sup>.

The reaction of iron aluminides with gases and sulfur present at high temperatures depends on the nature of the sulfur species present in the environment and the partial pressure of the oxygen in a particular atmosphere. For these materials, an alumina ( $\text{Al}_2\text{O}_3$ ) layer can be formed at very low oxygen pressures even in the presence of significant sulfur activity<sup>[5 and 6]</sup>. Nevertheless, iron-aluminum binary alloys with aluminum contents greater than 18 wt % continue having good resistance up to 750 °C<sup>[7-10]</sup>. At 750 °C and 900 °C, when exposed in sulfur vapor at  $10^{-30}$  Pa a  $\text{Fe}_3\text{Al}$  alloy with 28 wt % aluminum forms an external film of  $\text{Al}_2\text{S}_3$ , but at pressures higher than 133 Pa, the sulfidation rate increased quickly with time at 800 °C<sup>[11]</sup>.

Sulfur can coexist with oxygen, carbon, chlorine and hydrogen in many service atmospheres. As an example of this, in industrial process such as carbon gasification the sulfur partial pressure  $p(\text{S}_2)$  is high and the oxygen partial pressure  $p(\text{O}_2)$  is low<sup>[12]</sup>. Nevertheless, the oxygen potential is high enough to form  $\text{Al}_2\text{O}_3$  on alloys such as  $\text{Fe}_3\text{Al}$  and FeAl. On these, the corrosion behavior is controlled by the integrity and adherence of the alumina scale<sup>[13]</sup>. In other combustion processes, particularly in combustion power systems, the oxygen partial pressure  $p(\text{O}_2)$  in the environment is high and the sulfur partial pressure  $p(\text{S}_2)$  is low, in general, sulfur is present in the form of  $\text{SO}_2$ <sup>[14]</sup>.

In these conditions, iron aluminides tend to form a protective  $\text{Al}_2\text{O}_3$  layer, which can resist corrosion

under mixtures of sulfur and oxygen containing gases<sup>[6, 13-15]</sup>. FeAl and  $\text{Fe}_3\text{Al}$  alloys present better sulfidation resistance than Fe-Cr-Al alloys under the same conditions of gases with high  $p(\text{S}_2)$ -low  $p(\text{O}_2)$ . Chromium (Cr) in iron aluminides decreases the sulfidation resistance at 800 °C. However, the opposite is true if the chromium content is lower than 2 % or if the aluminum content increases (>12 wt % Al)<sup>[4]</sup>.

$\text{Fe}_3\text{Al}$  type intermetallics are widely used for their high temperature oxidation resistance due to their ability to develop an  $\text{Al}_2\text{O}_3$  protective layer, which also provides corrosion resistance in molten salts<sup>[13 and 16]</sup>. However, one of the main drawbacks for these aluminides is their poor ductility. Salazar *et al.*<sup>[17]</sup> found that alloying aluminides with either lithium, cerium or nickel results in an improvement of their ductility, and described the mechanical properties and microstructural features for these materials. Thus, the aim of this paper is to examine the effect of small additions of cerium, lithium and nickel on the corrosion behavior of  $\text{Fe}_3\text{Al}$  type intermetallics exposed to an  $\text{SO}_2+\text{N}_2$  environment at high temperature.

## 2. EXPERIMENTAL PROCEDURES

The materials used in this work were  $\text{Fe}_3\text{Al}$  intermetallics with additions of 1 at. % of lithium, cerium or nickel produced by conventional casting. The various alloys tested were  $\text{Fe}_3\text{Al}$ ,  $\text{Fe}_3\text{AlLi}$ ,  $\text{Fe}_3\text{AlNi}$ ,  $\text{Fe}_3\text{AlCeLi}$  and  $\text{Fe}_3\text{AlCeNi}$ . The dimensions of the samples were 5x5x3 mm. All the samples were polished with alumina powder of 1.0  $\mu\text{m}$ , degreased with acetone and dried under a stream of hot air. Finally, each sample was weighted in a microbalance with a resolution of  $10^{-5}$  g. The experimentation was carried out in a thermo-gravimetric apparatus (TGA) C. I. Mark2 CT5 in an atmosphere of 2.5 %  $\text{SO}_2+\text{N}_2$  with a flow rate of 50 cc/min and a temperature of 900 °C during 48 h. After testing, the samples surfaces were analyzed in a scanning electronic microscope (SEM) Jeol 5800LV and chemical microanalysis were carried out by using a X-ray energy dispersive spectroscopy unit (EDS, Mod. Genesis) attached to it.

## 3. RESULTS

The weight gain curves for the various intermetallics are shown in the figure 1.

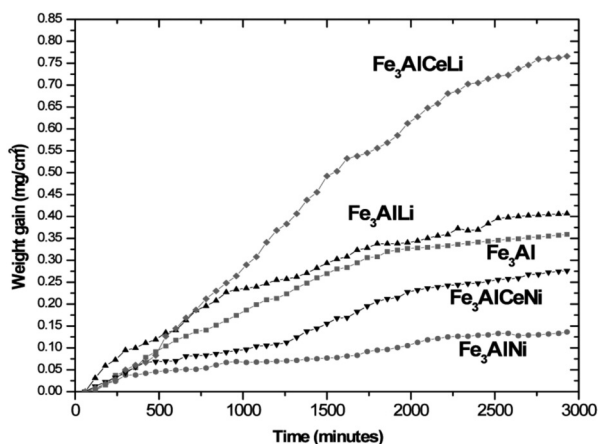


**Figure 1.** Weight change vs time for the various intermetallic alloys exposed to SO<sub>2</sub>+N<sub>2</sub> at 900 °C for 48 h.

*Figura 1. Cambio de peso vs tiempo para las diferentes aleaciones intermetálicas expuestas a SO<sub>2</sub>+N<sub>2</sub> a 900 °C durante 48 h.*

In general, for all the specimens the corrosion kinetics show a parabolic behavior with the Fe<sub>3</sub>Al, Fe<sub>3</sub>AlLi and Fe<sub>3</sub>AlCeNi disclosed somewhat similar weigh gain values after 3000 min (48 h). The lowest weight gain was recorded for the Fe<sub>3</sub>AlNi alloy whereas the Fe<sub>3</sub>Al+Ce+Li disclosed the highest weight gain value. In each case, duplicate runs were carried out and the reported data represent the average. The data were fitted to an equation of the form  $x = c t^b$ , where  $x$  is the weight gain per unit area and  $t$  is the time. A straight line on a log-log plot gives the value of  $b$  (slope). Clearly, a value of  $b=0.5$  represents a parabolic law. Hence, by force fitting the data to  $b=0.5$ , the parabolic rate constant,  $K_p$ , can be calculated, i.e. by plotting the square of the weight gain per unit area vs time, the slope of the linear portion gives the value of  $K_p$ . Table I shows the parabolic kinetic constants derived from the previous method for each alloy.

As mentioned above, the parabolic constant values confirm that the Fe<sub>3</sub>AlNi alloy showed the smaller corrosion rate. It would be important to make a correlation of the behavior of the present aluminides with other earlier studies. Nevertheless, it seems that this is not possible because the available data<sup>[18-25]</sup> on literature related to sulfidation studies of Fe-Al alloys are limited. In addition, experimental variables such as exposure time, different temperatures and differences regarding the environment (H<sub>2</sub>/H<sub>2</sub>S/H<sub>2</sub>O) used should be taken into account. Therefore, the corrosion behavior for the alloys in the present study cannot be compared directly with reports from the literature.

**Table I.** Parabolic kinetic constants for each of the alloys exposed in SO<sub>2</sub>+N<sub>2</sub> at 900 °C for 48 h

*Tabla I. Constantes de la cinética parabólica para cada una de las aleaciones expuestas en SO<sub>2</sub>+N<sub>2</sub> a 900 °C durante 48 h*

Intermetallic alloy	$k_p$ , mg <sup>2</sup> cm <sup>-4</sup> s <sup>-1</sup>
Fe <sub>3</sub> AlCeLi	1.86x10 <sup>-10</sup>
Fe <sub>3</sub> AlCeNi	2.34x10 <sup>-11</sup>
Fe <sub>3</sub> AlLi	5.83x10 <sup>-11</sup>
Fe <sub>3</sub> Al	4.69x10 <sup>-11</sup>
Fe <sub>3</sub> AlNi	5.91x10 <sup>-12</sup>

Figure 2 a) shows the morphology of corrosion products formed on the Fe<sub>3</sub>Al base alloy in plain view, where it can be noted small areas of oxide spallation.

EDS analysis of the scale,(Fig. 2 b)), showed that this layer consists mainly of aluminum and oxygen, i.e. possibly Al<sub>2</sub>O<sub>3</sub> with some traces of iron. A cross section view, (Fig. 2 c)), shows oxide detachment from the substrate. It is also possible to observe cracking of the oxide scale.

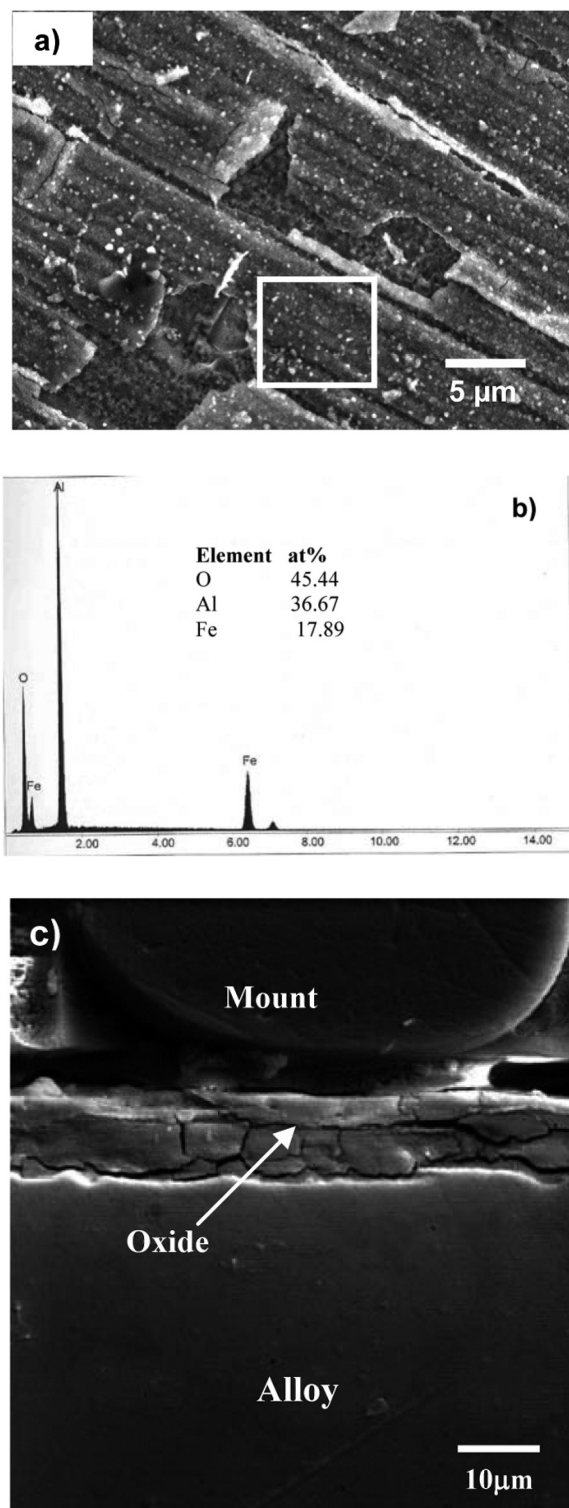
For the Fe<sub>3</sub>AlNi intermetallic alloy, a needle-like shrub of Al<sub>2</sub>O<sub>3</sub>, (Fig. 3 a)), covered the surface. EDS analysis of the scale showed that this layer is composed by aluminum and oxygen, possibly Al<sub>2</sub>O<sub>3</sub>, (Fig. 3 b)). Figure 3 c) shows the formation of microcavities located in the metal base/oxide scale interface.

Figure 4 shows excessive loosening of the formed oxide scale on the Fe<sub>3</sub>AlLi alloy. In addition, on the scale surface the development of needle-like shape transient oxides can be noted.

The scale developed on the Fe<sub>3</sub>AlCeNi alloy, (Fig. 5 a)), shows cracks and in some regions complete detachment to the substrate.

The loosening of the oxide scale allowed to observe the formation of microcavities located in the metal base/oxide scale interface (Fig. 5 b)). EDS analysis of the deposits showed that this layer is made mainly of aluminum and oxygen, possibly Al<sub>2</sub>O<sub>3</sub> with some traces of iron and sulfur (Fig. 5 c)).

A SEM image of the Fe<sub>3</sub>AlCeLi alloy shows a general aspect of the scale formed, which is not completely smooth. Instead, a convoluted scale structure containing fine needle-like alumina is noted. Locally, some cracks were found but there was no clear indication of spallation of part of the oxide scale (Fig. 6 a)). EDS analysis reveals the presence of aluminum and oxygen as main



**Figure 2.** a) SEM micrograph of the corrosion products formed on Fe<sub>3</sub>Al intermetallic alloy, b) EDS analysis on oxide scale taken in the area (square) shown in a) and c) cross section of a).

*Figura 2. a) MEB de los productos de corrosión formados sobre el intermetálico Fe<sub>3</sub>Al, b) análisis EDS en el área marcada en recuadro sobre la costra de óxido en a) y c) sección transversal de a).*

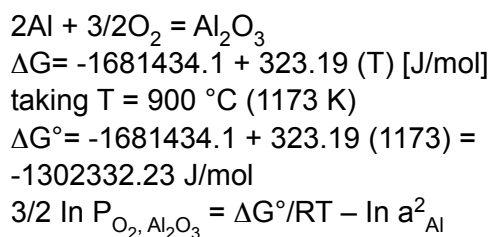
elements and some traces of iron and cerium (Fig. 6 b)).

A cross section view of the specimen, (Fig. 6 c)), shows that the oxide scale is very thin, less than 5 μm.

#### 4. DISCUSSION

Aluminum forms stable phases with oxygen, carbon, nitrogen and sulfur. Between 621 °C and 1093 °C, it can form three different sulphides, namely Al<sub>2</sub>S<sub>3</sub> (s), AlS (s, g) and Al<sub>2</sub>S (s, g). Free energy data for Al<sub>2</sub>S are not available and the limited data for the Al-S system suggested that Al<sub>2</sub>S<sub>3</sub> is the most stable phase ( $\Delta G_{\text{Al}_2\text{S}_3}^{1173\text{K}} = 338.2 \text{ kJ/mol}$ )<sup>[8]</sup>. Iron forms stable phases with oxygen, carbon, nitrogen and sulfur. Between 570 °C and 1093 °C, reacts with oxygen to form phases such as Fe<sub>0.95</sub>O (s), Fe<sub>3</sub>O<sub>4</sub> and Fe<sub>2</sub>O<sub>3</sub>, and with sulfur to form FeS<sub>1+x</sub> (s) and FeS<sub>2</sub> (s). Figure 7 shows the phase stability diagram for the Fe-Al-S-O system at 900 °C<sup>[26]</sup>.

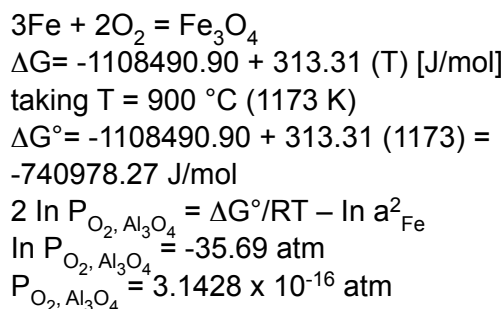
An atmosphere containing O<sub>2</sub>-SO<sub>2</sub> or a gas mixture of H<sub>2</sub>-H<sub>2</sub>O-H<sub>2</sub>S will generate oxygen and sulfur partial pressures high enough to support the formation of oxides and sulfides<sup>[27]</sup>. The activity of iron and aluminum in Fe-Al system are 0.217 and 0.022 at 900 °C (1173 K), respectively<sup>[28]</sup>. Taking data from NIST-JANAF<sup>[29]</sup> for the following reactions, we have:



$$\ln P_{\text{O}_2, \text{Al}_2\text{O}_3} = -83.934 \text{ atm}$$

$$P_{\text{O}_2, \text{Al}_2\text{O}_3} = 3.53 \times 10^{-37} \text{ atm}$$

Similarity



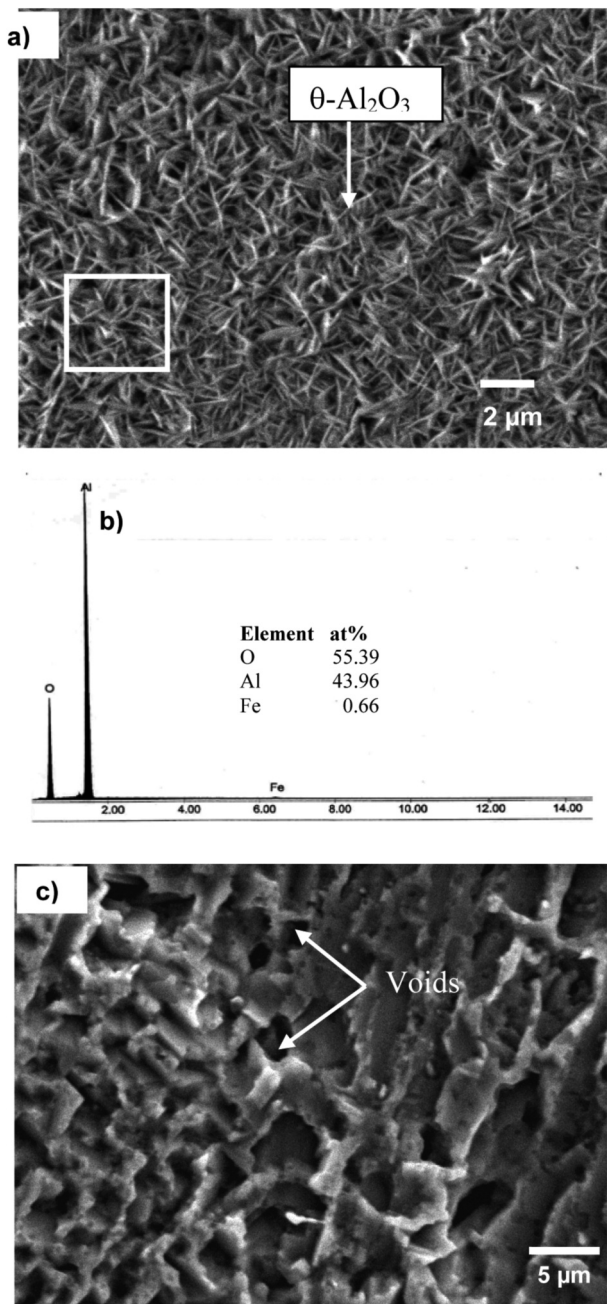


**Figure 3.** a) SEM micrograph of corrosion products formed on Fe<sub>3</sub>AlNi intermetallic alloy, b) EDS analysis on metastable  $\theta\text{-Al}_2\text{O}_3$  taken in the area (square) shown in a) and c) formation of voids in metal/scale interface.

*Figura 3. a) MEB de productos de corrosión formados sobre el intermetálico Fe<sub>3</sub>AlNi, b) análisis EDX tomado en el área marcada en recuadro sobre la alúmina metaestable mostrada en a) y c) formación de cavidades en la intercara metal base/costra.*

These calculations suggest that the formation of both Al<sub>2</sub>O<sub>3</sub> and Fe<sub>3</sub>O<sub>4</sub> are possible under the present

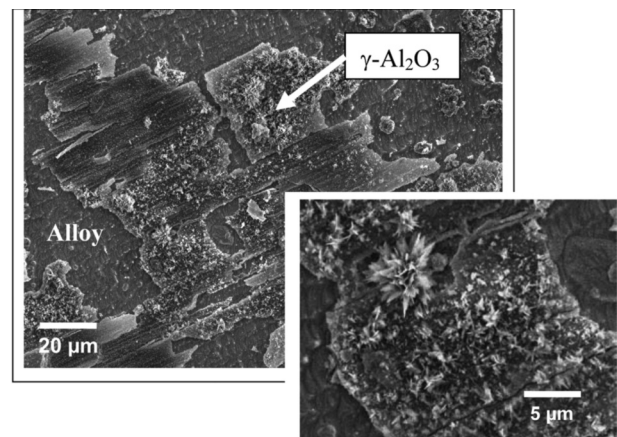


**Figure 4.** SEM micrograph of the corrosion products formed on Fe<sub>3</sub>AlLi intermetallic alloy. Significant area of bare metal is revealed by scale spallation.

*Figura 4. MEB de los productos de corrosión formados sobre el intermetálico Fe<sub>3</sub>AlLi. El descostamiento de óxido revela áreas de metal base.*

experimental conditions. In order to access the sulfur partial pressure pertinent to the present experimental conditions, we consider the reaction  $\text{SO}_2(\text{g}) \rightarrow \text{S}(\text{g}) + \text{O}_2(\text{g})$  at 900 °C (1173 K). At this temperature, the equilibrium constant  $k = 1.647 \times 10^{-19}$  is given by<sup>[26]</sup>:

$$k = \frac{[\text{S}] [\text{O}_2]}{[\text{SO}_2]} = \frac{x^2}{1-x} \quad (1)$$

where  $x$  is the degree of conversion. Solving the equation for  $x$  we obtain  $x = 4.059 \times 10^{-10}$ . This value indicates that, at equilibrium, the dissociation of SO<sub>2</sub> is very small. Thus, if the SO<sub>2</sub> partial pressure in the system is 0.025 atm, at equilibrium conditions  $P_{\text{S}} = 1.014 \times 10^{-11}$  atm and  $P_{\text{O}_2} = 1.014 \times 10^{-11}$  atm. Figure 7 shows these values on the Fe-Al-S-O phase stability diagram, from which it can be seen that the stable compounds are Al<sub>2</sub>O<sub>3</sub> and Fe<sub>3</sub>O<sub>4</sub>.

From the EDS analysis carried out on the surface of the Fe<sub>3</sub>Al, Fe<sub>3</sub>AlCeLi, Fe<sub>3</sub>AlNi and Fe<sub>3</sub>AlCeNi alloys, important amounts of aluminum, oxygen and iron were detected. This is in agreement with the phase diagram on figure 7, from which it can be seen that the scale is composed mainly of alumina (Al<sub>2</sub>O<sub>3</sub>), whereas the iron signal may correspond to magnetite, Fe<sub>3</sub>O<sub>4</sub>. Sulfur was not detected on the scale formed on the various intermetallic alloys, with the only exception being for the Fe<sub>3</sub>AlCeNi intermetallic. On this alloy, a small amount of sulfur at the metal/scale interface and on the surface was detected, for which, depending

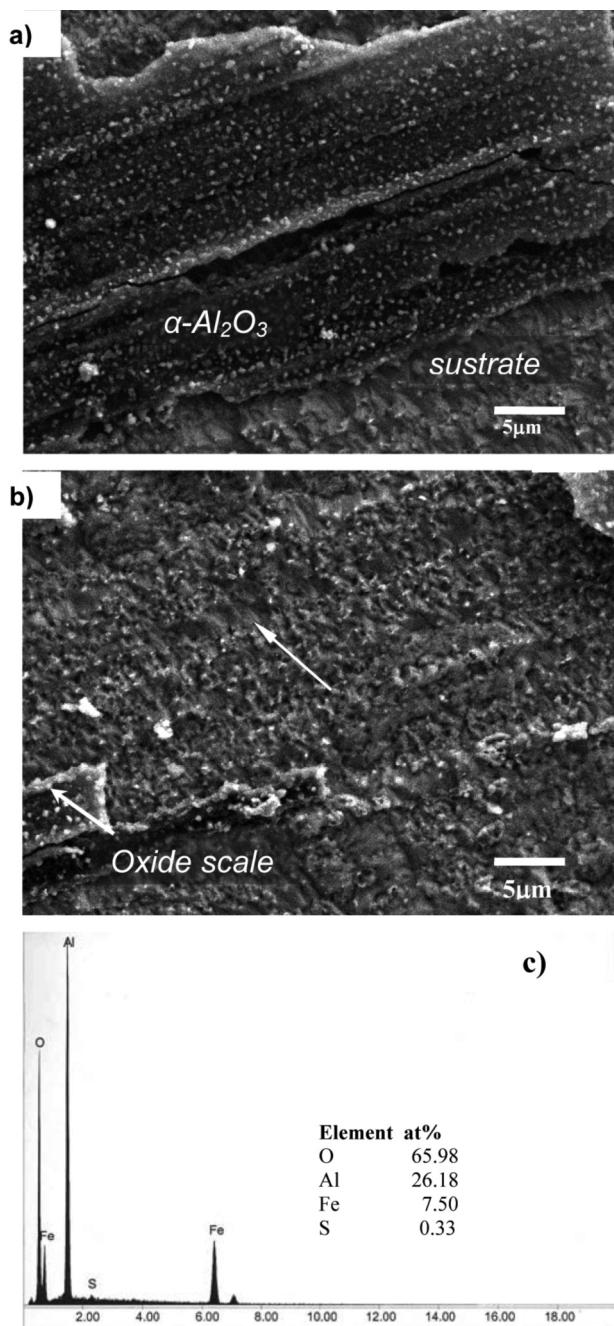


**Figure 5.** a) SEM micrograph of the corrosion products formed on  $Fe_3AlCeNi$  intermetallic alloy, b) formation of voids in matrix/scale interface and c) EDS analysis taken in the area (square) on oxide scale shown in a).

*Figura 5. a) MEB de los productos de corrosión formados sobre el intermetálico  $Fe_3AlCeNi$ , b) formación de cavidades en la interfase metal base/costra y c) análisis EDS en el área marcada en recuadro sobre la costra de óxido mostrada en a).*

upon the activity of sulfur or aluminum, sulfur can be associated with an aluminum sulfide such as  $(Al_2S_3)^{[30]}$

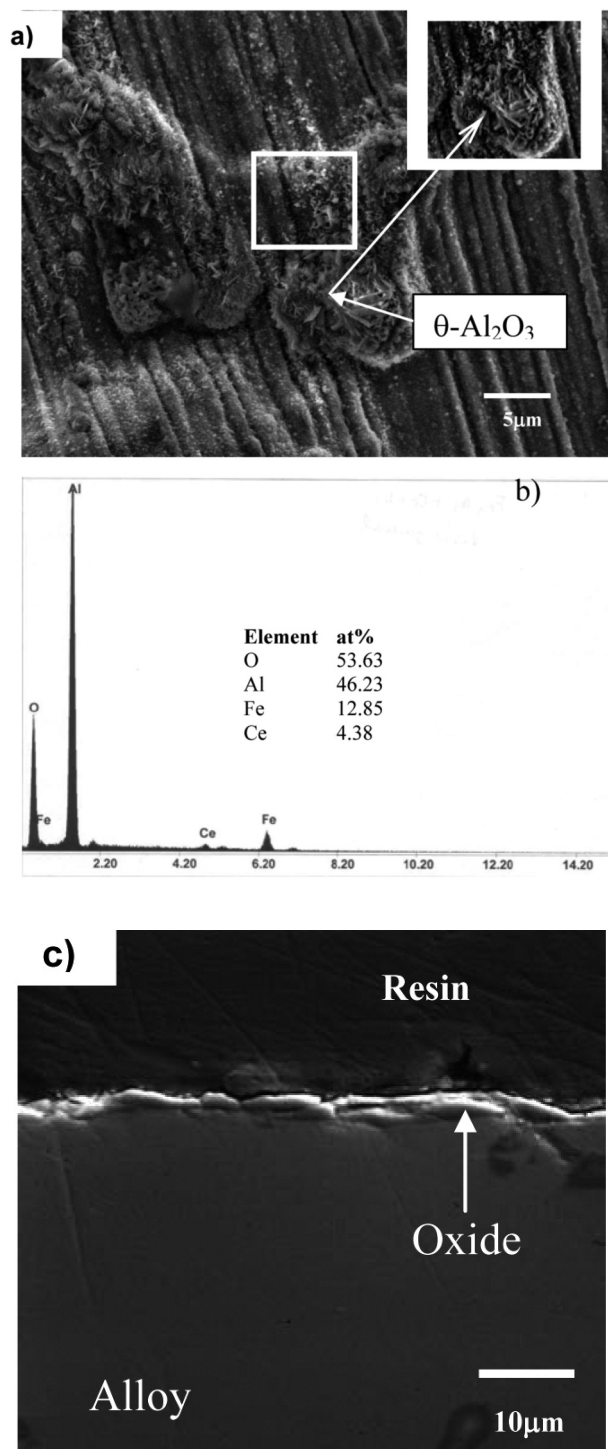


**Figure 6.** a) SEM micrograph of the corrosion products formed on  $Fe_3AlCeLi$  intermetallic alloy; b) EDS analysis taken in the area (square) shown in a) and c) cross-section of a).

*Figura 6. a) MEB de los productos de corrosión formados sobre el intermetálico  $Fe_3AlCeLi$ ; b) análisis EDS en el área marcada en recuadro en a) y c) sección transversal de a).*

or with an iron sulfide plus alumina ( $FeS+Al_2O_3$ )<sup>[5]</sup>. For the  $Fe_3Al + xCr$  ( $x=2\%$  and  $5\%$ ) it has been

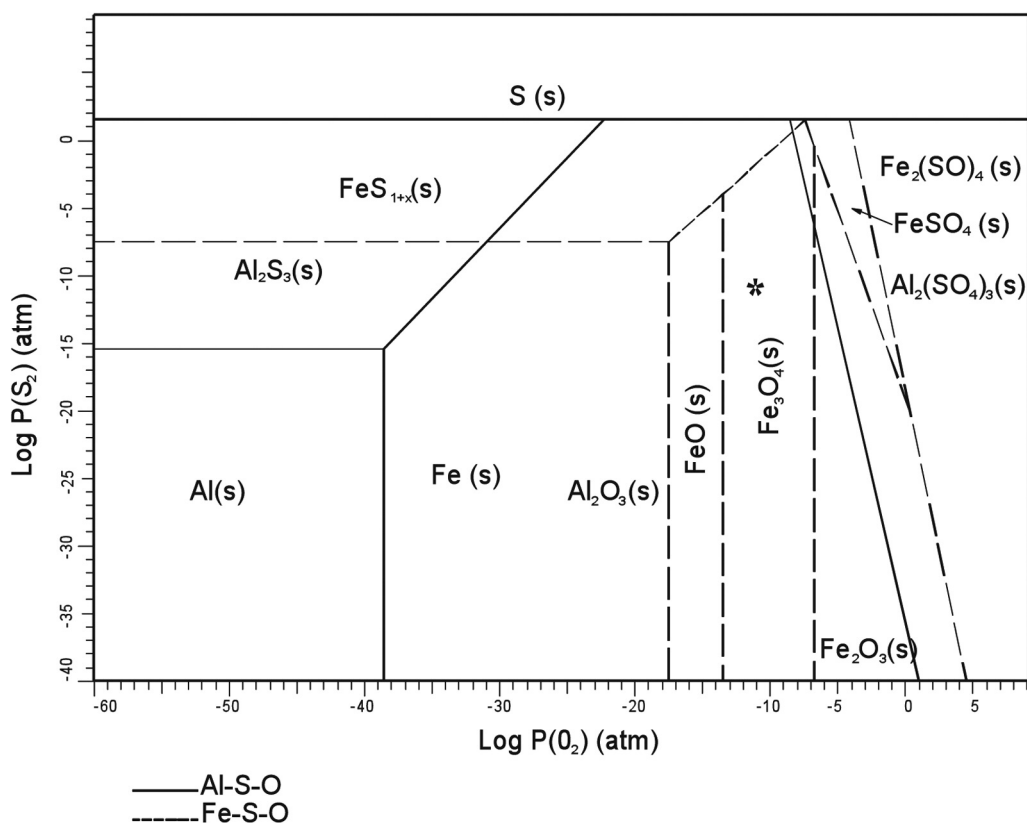


**Figure 7.** Phase stability diagram for Fe-Al-S-O system at 900 °C [26].  
 \* indicates the experimental conditions in this work.

**Figura 7.** Diagrama de estabilidad de fases para el sistema Fe-Al-S-O a 900 °C [26]  
 \* indica las condiciones experimentales en este trabajo.

reported that only a needle-shape Al<sub>2</sub>O<sub>3</sub> form in both air and 1 % SO<sub>2</sub>/air environments at 800 °C, although the formation of Al<sub>2</sub>S<sub>3</sub> traces has also been observed<sup>[31]</sup>.

The external scale formed on Fe<sub>3</sub>AlCeLi intermetallic alloy still shows some traces of a transient oxide that is characterized for having a platelet morphology. This morphology was observed between 800 °C and 950 °C, and generally contains high concentration of vacancies, which can lead to cavities nucleation<sup>[32]</sup>. The EDS analysis carried out on the external surface on this intermetallic indicated that mainly is Al<sub>2</sub>O<sub>3</sub>, whereas the iron detected indicates that the formation of an iron oxide would be possible. Small particles of cerium were detected, so the presence of this element indicates an outward cation migration and the presence of a cerium-containing oxide is possible.

#### 4.1. Effect of alloy additions

On the whole, the Fe<sub>3</sub>AlNi intermetallic alloy disclosed the smaller rate corrosion whereas the least

resistant was the Fe<sub>3</sub>AlCeLi alloy, this last in spite of being the less resistant in terms of weight gain, although the later did not show signs of detachment (Fig. 6). On the other hand, it has been reported<sup>[33]</sup> the positive effects given by addition of alloying elements in intermetallic compounds, as well as of the different mechanisms, which try to explain the effect of these elements. One of the main effects is to improve the scale adhesion by suppressing interfacial voids; for example, the presence of pores has been observed on alloys without addition of reactive elements such as yttrium, hafnium and zirconium<sup>[34]</sup>. Particularly, intermetallic alloys such as NiAl, FeAl and PtAl are susceptible to the formation of large cavities at the alloy/scale interface, for which the addition of alloying elements like cerium or lithium would help to suppress cavity formation.

The oxide scale formed on the Fe<sub>3</sub>Al, Fe<sub>3</sub>AlNi, Fe<sub>3</sub>AlLi and Fe<sub>3</sub>AlCeNi alloys was susceptible to the spalling, it could have been assisted or attributed by the difference of the thermal expansion coefficient between the base metal and oxide formed<sup>[35 and 36]</sup> as

well as the formation of microcavities<sup>[37]</sup> in the interface metal/oxide as happened in the intermetallic Fe<sub>3</sub>AlNi and Fe<sub>3</sub>AlCeNi.

The Fe<sub>3</sub>AlNi and Fe<sub>3</sub>AlLi intermetallics were particularly prone to the formation of transitory forms of alumina such as  $\gamma$ - $\theta$ -Al<sub>2</sub>O<sub>3</sub>. The morphology of these oxide phases is in a whiskers shape form ( $\theta$ -Al<sub>2</sub>O<sub>3</sub>) see figure 3, or platelets ( $\gamma$ -Al<sub>2</sub>O<sub>3</sub>) see figures 4 and 6, indicative of outward diffusion of Al<sup>3+</sup> ions; with the main factor promoting the formation of this oxide being the test temperature (900 °C)<sup>[38]</sup>. The literature available mention that temperatures below 1050 °C promotes its formation, although is also mentioned that this type of oxides is formed or is stable in the temperature range between 800 to 850 °C<sup>[8 and 28]</sup>. This is consistent with the morphology shown by the intermetallics with additions of lithium and nitrogen, but not for the Fe<sub>3</sub>AlCeLi intermetallic, which showed isolated zones of oxide with a platelet shape. This intermetallic showed a continuous, well-adhered scale, without detachments. Nevertheless, after 48 h, it disclosed the highest weigh gain values. Although this intermetallic shows an oxide scale without evidence of detachment, some cracks are clearly observed at the surface. Hence, easy access of oxygen towards the surface of the metal base is very likely generating an internal oxidation process. Thus, the recorded weight gain increased considerably with time.

EDS analysis on the surface of the oxide showed that its composition is entirely of alumina (Fig. 6 b)) which could be  $\alpha$ -Al<sub>2</sub>O<sub>3</sub>, since the transition from  $\gamma$ -Al<sub>2</sub>O<sub>3</sub> to  $\alpha$ -Al<sub>2</sub>O<sub>3</sub> occurs approximately at 900 °C<sup>[39]</sup>. Nevertheless, the small plates that are observed on the surface could be a metastable oxide such as  $\gamma$ -Al<sub>2</sub>O<sub>3</sub><sup>[38]</sup>. The combined effect of cerium plus lithium apparently contributed to the transition from  $\gamma$ -alumina to  $\alpha$ -alumina.

#### 4. CONCLUSIONS

- The corrosion kinetic data found for the various Fe<sub>3</sub>Al intermetallic alloys indicates that not all the alloying elements added to the base alloy were effective to improve the sulfidation resistance. The Fe<sub>3</sub>AlNi intermetallic alloy disclosed the highest sulfidation resistance, whereas the least resistant was the Fe<sub>3</sub>AlCeLi alloy.
- The corrosion products in the intermetallic alloys tested consisted mainly of Al<sub>2</sub>O<sub>3</sub>, some transient oxides such as  $\theta$  or  $\gamma$ -Al<sub>2</sub>O<sub>3</sub> and iron or aluminum sulfides.
- The addition of lithium, cerium and nitrogen did not show a consistent effect on the corrosion

behavior. The elements added to the intermetallic base alloy decreased the growth rate of the oxide scale, but did not improve the spalling. This problem was not solved by the addition of elements in the intermetallic alloy. Regarding void formation, the alloying elements did not have a positive effect, since the intermetallic alloys (Fe<sub>3</sub>AlNi and Fe<sub>3</sub>AlCeNi) developed cavities at the metal/scale interface.

#### Acknowledgements

The authors wish to thank the financial support given by the Consejo Nacional de Ciencia y Tecnología (CONACyT), México to carry out this work.

#### REFERENCES

- [1] *Metals Handbook* Ninth Edition, Vol. 13, *Corrosion, High-Temperature Corrosion in Gases*, ASM International, 1987, p. 97.
- [2] C. G. McKamey, J. H. Devan, P. F. Tortorelli and V. K. Sikka, *J. Mater. Res.* 6 (1991) 1779-1805.
- [3] V. K. Sikka, C.G. McKamey, C.R. Howell and R.H. Baldwin, *Fabrication and Mechanical Properties of Fe<sub>3</sub>Al-Based Aluminides*, ORNLRTM-11465, Oak Ridge National Laboratory, Oak Ridge, TN, 1990.
- [4] K. Natesan and P.F. Tortorelli, *Proc. Int. Symp. on Nickel and Iron Aluminides Processing, Properties, and Applications*, Cincinnati, OH, 1996, ASM International, Materials Park, OH, 1997, pp. 265-287.
- [5] J.H. Devan, H.S. Hsu and M. Howell, ORNL, report TM-11176, Oak Ridge, TN, 1989.
- [6] K. Natesan, *Mater. High Temp.* 14 (1997) 71-79.
- [7] K. N. Strafford and R. Manifold, *Oxid. Met.* 5 (1972) 85-112.
- [8] P. C. Patnaik and W.W. Smeltzer, *Oxid. Met.* 23 (1985) 53-75.
- [9] P. J. Smith and W.W. Smeltzer, *Oxid. Met.* 28 (1987) 291-297.
- [10] S. Mrowec, *Oxid. Met.* 44 (1995) 177-209.
- [11] P.C. Patnaik and W.W. Smeltzer, *J. Electrochem. Soc.* 132 (1985) 1226-1232.
- [12] V. L. Hill and H. S. Mayer, *High Temperature Corrosion in Energy Systems*, Ed by M. F. Rothman. The Metallurgical Society of the AIME, 1985, pp. 29-52.

- [13] P. F. Tortorelli and K. Natesan, *Mater. Sci. Eng. A* 258 (1998) 115-125.
- [14] K. Natesan and R. N. Johnson, *Proceedings of the 2nd International Conf. on Heat-Resistant Materials*, K. Natesan, P. Ganesan, G. Lai (Eds.) Gatlinburg, Tennessee, 1995, pp. 591-600.
- [15] P. F. Tortorelli and J.H. Devan, Chapter 3 in: G. Welsch, P. D. Desai (Eds.), *Oxidation and Corrosion of Intermetallic Alloys*, Metals Information Analysis Center, Purdue University, West Lafayette, IN, 1996.
- [16] P. F. Tortorelli and P. S. Bishop, *Environmental Effects on Advanced Materials*, R.H. Jhones and R.E. Ricker (Eds.), The Minerals, Metals and Materials Society, Warrendale, P.A., 1991, p. 91.
- [17] M. Salazar, A. Albitzer, G. Rosas and R. Pérez, *Mater. Sci. Eng. A* 351 (2003) 154-159.
- [18] P. F. Tortorelli and J. H. Devan, *Mater. Sci. Eng. A* 153 (1992) 573-577.
- [19] W. Kai, S. H. Lee, D. L. Chiang and J. P. Chu, *Mater. Sci. Eng. A* 258 (1998) 146-152.
- [20] W. Kai, M.T. Chang, C.D. Liu, D.L. Chiang and J. P. Chu, *Mater. Sci. Eng. A* 329-331 (2002) 734-744.
- [21] W. Kai and R.T. Huang, *Oxid. Met.* (1997) 48-59.
- [22] W. Kai, J. P. Chu, R. T. Huang and P. Y. Lee, *Mater. Sci. Eng. A* 239-240 (1997) 859-870.
- [23] F.H. Stott, K.T. Chuah and L. B. Bradley, *Oxidation of Intermetallics*, Eds. H. J. Grabke, M. Schutze, 1997, pp. 221-232.
- [24] K. Natesan, *Mater. Sci. Eng. A* 258 (1998) 126-134.
- [25] J. H. Devan and P. F. Tortorelli, *Corros. Sci.* 35 (1993) 1065-1071.
- [26] J. J. Ramos-Hernández, Tesis de Maestría, Facultad de Química-UNAM, 2009.
- [27] K. Natesan, *Prepared for Environmental Degradations of High-Temperature Materials*, ANL, Argonne, Illinois, 1980, pp. 60-69.
- [28] A.K. Misra, *Thermodynamic Analysis of Compatibility of Several Reinforcement Materials With FeAl Alloys*. NASA Contractor Report 4172, 1988.
- [29] INS NIST-JANAF *Thermochemical Tables*, Fourth Edition, National Institute of Standards and Technology, 1998.
- [30] D.P. Whittle, *High Temp. Corros.* Ed. R. A. Rapp, NACE-6, Houston, 1981.
- [31] W. H. Lee and R. Y. Lin, *Mater. Chem. Phys.* 58 (1999) 231-242.
- [32] D. Monceau and B. Pieraggi, *Oxid. Met.* 50 (1998) 477-493.
- [33] P.L. Hemmings and R. A. Perkins, FP-539 Research Project 716-1. Prepared by EPRI, Palo Alto Cal. Dec. 1977.
- [34] K. Natesan, K. Klug, D. Renusgh, B. W. Veal and M. Grimsditch, ANL/FE-96/01, pp. 1-20.
- [35] B. A. Pint, *Mater. Sci. Forum.* 369-372 (2001) 411-418.
- [36] M. A. Montealegre and J. L. González-Carrasco, *Intermetallics* 11 (2003) 169-175.
- [37] D.B. Lee, G. Y. Kim and J. G. Kim, *Mater. Sci. Eng. A* 339 (2003) 109-114.
- [38] M.W. Brumm and H. Grabke, *J. Corros. Sci.* 33 (1992) 1667-1675.
- [39] P.F. Tortorelli and J. H. Devan, *Oxidation and Corrosion of Intermetallic Alloys*, Chapter 3. Ed. Welsh and P. D. Desai, 1996, pp. 266-321.